

56-33
198556

P-16

N94-23262

Cryogenic, Low-Noise High Electron Mobility Transistor Amplifiers for the Deep Space Network

J. J. Bautista

Radio Frequency and Microwave Subsystems Section

The rapid advances recently achieved by cryogenically cooled high electron mobility transistor (HEMT) low-noise amplifiers (LNAs) in the 1- to 10-GHz range are making them extremely competitive with maser amplifiers. In order to address future spacecraft navigation, telemetry, radar, and radio science needs, the Deep Space Network is investigating both maser and HEMT amplifiers for its Ka-band (32-GHz) downlink capability. This article describes the current state of cryogenic HEMT LNA development at Ka-band for the DSN. Noise performance results at S-band (2.3 GHz) and X-band (8.5 GHz) for HEMTs and masers are included for completeness.

I. Introduction

A key figure of merit in the specification of the communications link to a deep space mission is the ratio of the gain of the ground-based antenna divided by the system noise temperature (G/T_{sys}). The low-noise amplifier addresses the need to keep the system noise temperature as low as technology permits. Of secondary concern is the provision of broad bandwidth and high gain. Cryogenically cooled amplifiers using masers and high-electron mobility transistors (HEMTs) are employed by the DSN to meet these needs.

Historically, the extraordinarily sensitive receiver systems operated by the DSN have employed ruby masers as the low-noise front-end amplifier [1]. The rapid advances recently achieved by cryogenically cooled HEMT low-noise amplifiers (LNAs) in the 1- to 10-GHz range are making them extremely competitive with maser amplifiers [2,3]. In order to address its future navigation, telemetry, radar, and radio science needs, the DSN is investigating both

maser [4] and HEMT amplifiers for its 32-GHz downlink capability.

The telemetry needs at 32 GHz are best met with the lowest noise devices. For bandwidths of less than 400 MHz, maser noise temperatures at this frequency are expected to continue to outperform HEMT noise temperatures. On the other hand, the maser's instantaneous bandwidth is considerably smaller than the HEMT's. Thus, future requirements for large bandwidths, such as interferometric techniques for navigation or for radio astronomy, are more likely to be met with HEMT LNAs. In addition, the use of follow-up HEMT amplifiers reduces the gain requirements for the maser, permitting wider maser bandwidths.

II. Cryogenic Cooling

Cryogenic cooling is applied to a variety of low-noise microwave receivers, such as field-effect transistor (FET) and HEMT amplifiers, mixers, upconverters, parametric

amplifiers, and masers, to reduce thermal noise. To provide physical temperatures down to 4.5 K, commercially available helium closed-cycle refrigerators (CCRs) are usually employed. For temperatures below 4.5 K, a pumped, open cycle liquid helium bath, or hybrid CCR with liquid bath, is used. In the hybrid system, the CCR is used to cool radiation heat shields in order to conserve liquid helium. To obtain the lowest possible noise temperatures, as many as are physically possible of the input and output rf components are cooled below ambient. Currently, the DSN relies on helium CCRs to provide the needed cryogenic temperatures [5].

Maser amplifiers provide the best possible telemetry support for deep space missions. However, these systems operate at a physical temperature of 4.5 K, requiring complex and expensive cryogenic systems. HEMT LNAs, on the other hand, require less cooling power and operate at a higher physical temperature of 12 K, where more cooling power is available. At this higher temperature, a less complex (less expensive) and more reliable refrigeration system can be used. The lower cost of HEMT LNAs will lead to greater frequency coverage and the economic realization of multiple-element room-temperature and/or cryogenic array feed systems. For example, in preparation for Voyager's encounter with Neptune in 1989, JPL planned to array the DSN Goldstone antenna complex with the National Radio Astronomy Observatory (NRAO) Very Large Array (VLA) in Socorro, New Mexico. It cost eight million dollars to equip the 27 VLA antennas with 8.4-GHz HEMT/CCR receivers. To equip the VLA with maser/CCR receivers would have cost approximately 25 million dollars.

Cooling below 4.5 K can result in significant performance improvements for masers, but not for HEMTs. Immersing a maser LNA in a bath of superfluid helium (2.2 K) achieves more than just an improved thermal contact. The gain of a maser in decibels increases in inverse proportion to the physical temperature, while the noise temperature decreases in direct proportion to it. For example, on cooling an 8.4-GHz maser from 4.5 to 1.6 K, the gain in decibels increases threefold, while the noise temperature decreases by a factor of three. Figure 1 shows the noise temperature for physical temperatures from 4.6 to 1.6 K [6].

The noise temperature and gain of a HEMT, on the other hand, are relatively independent of temperature below 12 K.¹ Noise temperature measurements at 8.4 GHz

¹ J. J. Bautista and G. G. Ortiz, "HEMT Noise at 1.6 K," submitted to the *Journal of the Electrochemical Society*.

of a three-stage HEMT amplifier in liquid helium from 4.2 to 1.6 K are displayed in Figs. 2 and 3. The results show that the amplifier noise temperature of 5.45 K remains constant on cooling from 4.2 K to the lambda point (2.2 K), decreases abruptly to 5.25 K, and remains constant on further cooling from 2.2 to 1.6 K (the accuracy for these measurements was ± 0.1 K). The gain was observed to remain constant throughout the temperature range. Measurements of a two-stage 32-GHz HEMT LNA exhibited similar behavior under the same physical conditions.

Sub-4-K temperature operation is easier to attain in an open helium bath system than in a closed-cycle one. Although sub-4-K physical temperatures are very difficult to implement in a Cassegrain antenna, the laboratory-like environment of a beam-waveguide antenna will allow the implementation of a liquid helium open bath system. In a tipping environment, large (more than 20 deg from zenith) changes in orientation cause significant thermal load increases, resulting in noise temperature increases and reduced operating times. Although the maser will clearly benefit from the advent of beam-waveguide antennas, further understanding of the noise limitations in HEMT devices will result in the development of devices that continue to improve, decreasing to liquid helium temperatures.

III. Noise Fundamentals: Parameters and Models

For purposes of circuit modeling and device characterization, any noisy linear two-port device can be represented as a noiseless linear two-port device with the noise sources at the input and/or output [7,8]. Depending upon the utility of the representation, the internal (voltage and/or current) noise sources can be placed at the input or output port of the noiseless network. Figure 3 shows a convenient representation that leads to four noise parameters (T_{min} , R_{opt} , X_{opt} , and R_n) that can be determined from the measurement of noise temperature as a function of input match. It consists of a series noise voltage (e_n) and shunt noise current (i_n) source at the input [9]. In this representation, the two-port device's noise parameters are given by the equivalent noise resistance

$$R_n = \frac{\langle |e_n|^2 \rangle}{4kT_oB}$$

the noise conductance

$$g_n = \frac{\langle |i_n|^2 \rangle}{4kT_oB}$$

and the correlation coefficient

$$r = \frac{\langle e_n i_n \rangle}{\sqrt{\langle e_n^2 \rangle \langle i_n^2 \rangle}}$$

where $T_o = 290$ K, k is Boltzmann's constant, and B is the noise bandwidth.

The noise temperature (T_n) of the two-port device driven by a generator impedance Z_g is given by the expression

$$T_n = T_{min} + \frac{T_o g_n}{R_g |Z_g - Z_{opt}|^2}$$

where Z_{opt} is the optimal generator impedance that yields a minimum noise temperature and $Z_g = R_g + jX_g$ is the generator impedance. The relationship between the first set of noise parameters and those in the above expression is given by the following equations

$$X_{opt} = \frac{Im(C)}{g_n}$$

$$R_{opt} = \sqrt{R_n/g_n - X_{opt}^2}$$

$$T_{min} = 2T_o [g_n R_{opt} + Re(C)]$$

where

$$C = r \sqrt{R_n g_n}$$

In principle, the above noise parameters (Z_{opt} , T_{min} , and R_n) for FET and HEMT devices can be determined by measuring the noise temperature for four or more different known source impedances at a given frequency. However, since there are errors associated with the source impedance and the noise temperature measurements, additional measurements are usually taken to improve the statistics. The noise parameters, along with the scattering parameters, can then be utilized for the optimum design of an amplifier circuit.

The most often used model for device and circuit optimization is the semi-empirical one developed by Fukui [10]. In this model, the noise parameters are simple functions of the equivalent small-signal circuit elements (transconductance, g_m , gate-to-source capacitance, C_{gs} , and source and

gate resistances, r_s and r_g) at a given frequency. These circuit elements are in turn analytic functions of the device's geometrical and material parameters. The semiempirical approach of Fukui yields the following expressions for the noise parameters

$$T_{min} = \frac{k_1 \omega T_o C_{gs} \sqrt{(R_g + R_s)/g_m}}{2\pi}$$

$$R_n = \frac{k_2}{g_m}$$

$$R_{opt} = k_3 (1/4g_m + R_g + R_s)$$

$$X_{opt} = \frac{2\pi k_4}{\omega C_{gs}}$$

where k_1 , k_2 , k_3 , and k_4 are fitting factors that are determined experimentally. Although this model is widely used by device designers and served to guide the development of the first cryogenic HEMT devices for the Voyager 2 encounter with Neptune, the model provides very little insight into the physics of noise in HEMTs and FETs.

Considerable research has been conducted in the area of noise performance of field-effect transistors over the last two decades. Currently, however, a noise model which is useful for both device optimization and circuit design is not available.

A good noise model must agree with measurements and accurately predict noise parameters. The more recent analytical models that consider fundamental semiconductor steady-state transport properties only treat thermal noise within the channel. These are progressively more complex treatments of van der Ziel's original work [11,12]. The numerical noise model approach taken by Cappy et al. [13] takes into account electron dynamics and appears to explain noise temperature results. However, the dependence of the measured noise temperature on device parasitics and input circuit impedance complicates the full evaluation of numerical models.

A potentially powerful approach for submicron gate-width cryogenic device development would be a synthesis of M. Pospieszalski's frequency- and temperature-dependent circuit model [14] and Joshin's one-dimensional electron transport noise model [15].

Pospieszalski's model uses simple (small signal) circuit concepts that yield closed-form expressions for the noise

parameters. This model introduces frequency-independent equivalent temperatures for the intrinsic gate resistance (T_g) and drain conductance (T_d). The equivalent noise model for an intrinsic chip device is shown in Fig. 4. For low frequencies, that is for $\omega/\omega_t \ll \sqrt{(T_g/T_d)(1/r_{gs}g_{ds})}$ and $R_{opt} \gg r_{gs}$, the noise parameters are given by the following expressions

$$R_{opt} = \frac{\omega_t}{\omega} \sqrt{\frac{r_{gs}T_g}{g_{ds}T_d}}$$

where

$$\omega_t = \frac{g_m}{C_{gs}}$$

$$X_{opt} = \frac{1}{\omega C_{gs}}$$

$$T_{min} = \frac{2\omega}{\omega_t} \sqrt{g_{ds}T_d r_{gs}T_g}$$

and

$$g_n = \frac{T_{min}}{2R_{opt}T_o}$$

The utility of this model is that it allows the prediction of the noise parameters for a broad frequency range from a single frequency noise-parameter measurement at a given temperature.

In Joshin's microscopic model [15], the intrinsic gate and drain noise generators are derived from the physical properties of the GaAs semiconductor at ambient. By adding a physical temperature dependence to Joshin's model, it may be possible to predict and calculate the noise parameters directly from the physical properties of the semiconductor materials. Most models are not applicable at cryogenic temperatures and have shown limited agreement with room-temperature measurements. In any case, it is clear that much experimental and theoretical work remains before the HEMT device is optimized and exploited for cryogenic LNA applications.

IV. HEMT Devices

The HEMT is essentially a high-performance GaAs FET with a more detailed and layered active material

structure. Although the HEMT structure has many similarities to a conventional GaAs FET, different physical mechanisms control or limit the carrier transport properties in the region between the source and the drain. The conventional device structure shown in schematic cross-section in Fig. 5. is grown in layers on a GaAs substrate. First, to inhibit impurity diffusion into the active region, a 1- μm -thick buffer of GaAs is grown on a semi-insulating GaAs wafer. A spacer layer of AlGaAs from 20 to 60 Å is grown to reduce dopant donor ion/conduction electron interactions. Next a 300- to 400-Å AlGaAs layer doped with silicon atoms is grown. Finally, a heavily doped AlGaAs layer 450-Å thick is grown to provide ohmic contacts. This layered structure produces a conduction band discontinuity that forms a triangular one-dimensional quantum well at the AlGaAs heterojunction. Electrons from the AlGaAs layer are attracted to and collect at the one-dimensional conduction band minimum in the vertical direction on the GaAs side of the heterojunction, forming a two-dimensional electron gas in a plane normal to the vertical direction.

The primary advantage of this heterojunction structure is that, unlike the heavily doped channel of a conventional GaAs FET, there are significantly fewer impurities in the undoped GaAs where the two-dimensional electron gas resides. The result is that electrons experience fewer scattering events and thus travel at higher saturated velocities than in conventional FETs. The additional spatial separation provided by the spacer layer of the channel electrons from their parent ions results in enhanced electron mobility. At room temperature, HEMT mobility is more than a factor of two greater than the FET's, while at cryogenic temperatures its mobility is more than two orders of magnitude greater than the FET's.

Additional device enhancements currently being investigated are new materials with higher intrinsic mobility (e.g., InGaAs and InP), shorter gate lengths ($<0.10 \mu\text{m}$) to further reduce scattering events, and alternate doping strategies such as planar doping (i.e., confining the dopants to an atomic plane) for stronger carrier confinement.

The three-terminal device is completed with the fabrication of a Schottky-barrier gate which controls the number of electrons in the two-dimensional electron gas. In addition to a lower noise figure than for a GaAs FET, the HEMT also has several other inherent characteristics that make it more attractive for low-noise amplifiers. The scattering parameters (S-parameters) of a HEMT in a 50-ohm impedance circuit exhibit lower output return loss (S_{22}) and higher gain (S_{21}) than a GaAs FET of the same dimensions. This results in an inherently

better output match and larger gain-bandwidth product. The HEMT also has much lower noise conductance, g_n , and X_{opt} (where $Z_{opt} = R_{opt} + jX_{opt}$ is the optimum source impedance) than the comparable metal semiconductor FET (MESFET), resulting in a lower noise temperature over a broader bandwidth. In addition, its performance improves more rapidly with cooling than that of the GaAs FET. Figure 6 shows the noise temperature response comparison for a FET and HEMT at 8.4 GHz, as a function of physical temperature.

V. Device Characterization

Since one of the primary functions of the LNA is to minimize the receiver system noise temperature, the characterization and selection of HEMT devices is critical to LNA performance. The selection of the 0.25- μm gate length conventional AlGaAs/GaAs HEMTs for the 32-GHz LNAs was based on its previously demonstrated reliability and exceptionally high-gain and low-noise characteristics [16,17] at 8.4 GHz. The selected device gate width of 75 μm was determined by the trade-offs associated with optimum impedance matching, circuit bandwidth, intermodulation distortion, power handling capability, and power dissipation.

The devices were fabricated on selectively doped AlGaAs/GaAs heterostructures grown by molecular beam epitaxy (MBE) with a Varian GEN II system on a 3-in.-diameter GaAs substrate. The details of the material growth conditions are discussed elsewhere [18]. The HEMT wafer exhibited a sheet carrier density of $8.1 \times 10^{12}/\text{cm}^2$ with a mobility at 77 K of more than 75,000 cm^2/Vsec . All levels were defined by electron beam lithography, and the T-shape gates were fabricated using a tri-layer resistance technique [19] to achieve a low series gate resistance.

For low-noise performance at cryogenic temperatures, the HEMT device must exhibit good pinch-off characteristics and high transconductance, g_m . Good pinch-off characteristics are achieved by strong confinement of the charge carriers to the channel region, with a sharp interface of high quality and a large conduction band discontinuity. An enhanced g_m at the operating bias is obtained by judicious choices for doping concentration and space layer thickness [20]. An Al mole fraction of approximately 30 percent is required for a large conduction band discontinuity, while the high g_m is achieved with a 40- \AA space layer and a doping concentration of approximately $2 \times 10^{18}/\text{cm}^3$. Although these values result in a high-performance room-temperature device, at physical temperatures below 150 K

the device suffers from IV (current voltage) collapse [21] and exhibits the persistent photoconductivity effect associated with the presence of deep donor traps (so called DX centers). In order to obtain excellent device performance at cryogenic temperatures and to eliminate light sensitivity, previous work [2,20] has demonstrated that the Al composition must not exceed 23 percent, and the doping concentration must equal approximately $1.0 \times 10^{18}/\text{cm}^3$.

The data shown in Table 1, comparing two HEMTs with the same Al mole fraction (23 percent) but different doping concentrations in the n-AlGaAs layer, serve to illustrate the difference between low temperature and room-temperature device optimization. Device A has an n-AlGaAs doping concentration of $1.0 \times 10^{18}/\text{cm}^3$, while that of B is two times higher. As expected, at ambient, device B exhibited a higher g_m and associated gain than device A, with approximately the same noise figure for both devices. However, at a physical temperature of 13 K and 8.5 GHz, device B exhibited a minimum noise temperature of 13.1 K, while device A yielded a value of 5.3 K. These results illustrate that cryogenic measurements must be carried out in order to verify the device's noise performance.

VI. LNA Design Approach

A semiempirical method was utilized to obtain minimum noise temperature performance of the 0.25- by 75- μm devices [22]. A two-stage LNA fixture was used to perform the noise characterization of the devices at cryogenic temperatures. The two-stage LNA fixture was designed to achieve the best room temperature low-noise performance based on the measured room-temperature device parameters. Following construction and room-temperature optimization, the LNAs are biased for lowest noise performance at cryogenic temperatures. This approach was chosen for two important reasons. First, a cryogenic noise-parameter measurement system was still under development for frequencies from 26 to 40 GHz and was not available for these measurements. Second, since the device processing was uniform across the wafer and device gains varied from 5 to 8 dB, two cascaded identical devices were required to reduce the noise temperature contribution of the room-temperature noise measurement receiver.

The LNA fixture oxygen-free high-conductivity (OFHC) copper and dc bias circuits [23] are designed for operation at cryogenic temperatures. Diode protection was included in both the gate and drain bias circuits. Light-emitting diodes (LEDs) were mounted on the cover of the fixture above each of the HEMTs for the purpose

of examining their light sensitivity at cryogenic temperatures. The input and output ports utilize a broadband-WR28 to stepped-ridge-waveguide to microstrip transition. The dimensions of the transition are detailed in Fig. 7. Figure 8 shows the insertion loss and return loss of a stepped-ridge fixture that consists of two stepped-ridge transitions connected back-to-back with a half-inch long microstrip 50-ohm line. The input and output matching networks were designed based on the device equivalent circuit values obtained from fitting measured S-parameters at the low-noise bias condition to the model from 2 to 20 GHz at room temperature. The noise parameters are then calculated from the small signal circuit elements using the previously noted Fukui expressions. Input, output, and interstage matching circuits were designed on 10-mil quartz substrate with TaN thin film resistors and TiWAl metallization. A schematic diagram of the two-stage hybrid HEMT LNA is shown in Fig. 9. The edge-coupled symmetric microstrip dc-blocking transmission line also served as a bandpass filter, improving the out-of-band stability. The three- and four-stage LNAs are constructed from the two-stage by the insertion of additional interstage matching circuits.

VII. LNA and Radiometer Performance

The two- and three-stage LNAs were first measured at room temperature with the devices biased for lowest noise at room temperature and then biased for lowest noise performance at cryogenic temperatures. Both LNAs exhibited an average noise figure of approximately 2 dB from 28 to 36 GHz. From 29 to 34 GHz, the gains measured approximately 17 and 23 dB for the two-stage and three-stage LNAs, respectively. The addition of an external isolator only slightly (0.3 dB) degraded the gain and noise figure.

With the devices biased for lowest noise at cryogenic temperature (12 K), the noise temperature (referenced at the room-temperature input waveguide flange) of both LNAs was observed to decrease nearly quadratically as a function of physical temperature as they cooled from 300 to 12 K. The noise temperature of the two-stage LNA decreased from 350 K at ambient to 35 K at 14.5 K, while that of the three-stage LNA decreased from 400 to 41 K at 12.5 K (see Fig. 10). Figure 11 shows the cryogenic noise temperature and gain response from 31 to 33 GHz, along with bias settings for the three-stage LNA. At 32 GHz, the two-stage LNA noise temperature measured 35 K, with an associated gain of 16.5 dB, at a physical temperature of 14 K, while the three-stage LNA yielded a value of 41 K with 26.0-dB associated gain. It is also noted that the three-stage LNA displayed an almost flat noise tempera-

ture response across the measurement band with a minimum noise temperature of 39 K at 32 GHz, while the two-stage LNA displayed a noise temperature response monotonically decreasing from 31 to 33 GHz with a minimum noise temperature of 31 K at 33 GHz.

It was further observed that neither amplifier showed a persistent photoconductivity effect. That is, it was found that these devices can be cooled with or without illumination and/or dc bias, without any observable effect on the cryogenic low-noise performance.

Two 32-GHz cryogenic HEMT radiometers were developed employing four-stage LNAs based on the two- and three-stage LNA results. Figure 12 shows a picture of the four-stage LNA; its cryogenic gain and noise performance are plotted in Fig. 13. The first system, pictured in Fig. 14, is a total power radiometer that exhibited an input noise temperature referenced to the input room-temperature flange of 45 K. Its noise temperature and gain response as functions of frequency are plotted in Fig. 15. The other system, shown in Fig. 16 without its vacuum jacket and radiation shield, is a Dicke-switching radiometer which demonstrated an input noise temperature referenced to the horn aperture of 59 K. The noise temperature response as a function of frequency is plotted in Fig. 17.

VIII. Conclusion

Since the invention of the HEMT device in 1983, noise temperatures and device yields have steadily improved. Using devices with 0.25- μm gates produced by electron beam lithography, key parameters of the device structure, such as the thicknesses and doping semiconductor layers, have been systematically optimized for cryogenic operation. Figure 18 summarizes the evolution of performance improvement for both maser and HEMT amplifier systems over the past 25 years. When cooled to 15 K, the best device noise temperatures at 8.4 GHz were improved steadily from 8.5 K in 1985 to 5.3 K in 1987.

The results of the cryogenic coolable state-of-the-art 32-GHz HEMT LNAs and radiometers clearly demonstrate their potential to meet the future space science needs of the DSN. Currently, JPL is investigating 0.1- μm gate lengths and promising alternate structures (planar doped and single and double heterojunction) and materials (InGaAs and InP). Further advances in HEMT technology [24,25] promise to lead to improved performance at all frequencies and to make possible the development of amplifiers above 100 GHz.

References

- [1] S. M. Petty and D. L. Trowbridge, *Low Noise Amplifiers in the Deep Space Network—A Radio Communications Instrument for Deep Space Exploration*, JPL Publication 82-104, Jet Propulsion Laboratory, Pasadena, California, pp. 4-1-4-32, July 1983.
- [2] M. W. Pospieszalski, S. Weinreb, P. C. Chao, U. K. Mishra, S. C. Palmateer, P. M. Smith, and J. C. M. Hwang, "Noise Parameters and Light Sensitivity of Low-Noise High-Electron-Mobility Transistors," *IEEE Trans. Electron Devices*, vol. ED-33, pp. 218-223, 1986.
- [3] S. Weinreb, M. W. Pospieszalski, and R. Norrod, "Cryogenic, HEMT, Low-Noise Receivers for 1.3 to 43 GHz Range," *1988 IEEE MTT-S Digest*, pp. 945-948, 1988.
- [4] J. Shell and D. Neff, "A 32-GHz Reflected Wave Maser Amplifier with Wide Instantaneous Bandwidth," *1988 IEEE MTT-S Digest*, pp. 789-792, 1988.
- [5] W. H. Higa and E. Wiebe, "One Million Hours at 4.5 Kelvin," *Proc. App. of Closed-Cycle Cryocoolers to Small Superconducting Devices*, Boulder, Colorado, pp. 99-108, October 1978.
- [6] D. L. Johnson, S. M. Petty, J. J. Kovatch, and G. W. Glass, "Ultralow Noise Performance of an 8.4-GHz Maser-Feedhorn System," *The Telecommunications and Data Acquisition Progress Report 42-100, vol. October-December 1989*, Jet Propulsion Laboratory, Pasadena, California, pp. 100-110, February 15, 1990.
- [7] IRE Subcommittee 7.9 on Noise, "Noise Representation of Noise in Linear Two Ports," *Proc. IRE*, vol. 48, pp. 69-74, January 1960.
- [8] H. Rothe and W. Dahlke, "Theory of Noisy Fourpoles," *Proc. IRE*, vol. 44, pp. 811-818, June 1956.
- [9] P. Penfield, "Wave Representation of Amplifier Noise," *IRE Circuit Theory*, vol. CT-9, pp. 84-86, March 1962.
- [10] H. Fukui, "Design of Microwave GaAs MESFETs for Broadband, Low-Noise Amplifiers," *IEEE Trans. Microwave Theory Tech.*, vol. MTT-27, pp. 643-650, July 1979.
- [11] A. van der Ziel, "Thermal Noise in Field-Effect Transistors," *Proc. IRE*, vol. 50, pp. 1808-1812, 1986.
- [12] A. van der Ziel, "Gate Noise in Field-Effect Transistors at Moderately High Frequencies," *Proc. IRE*, vol. 51, pp. 461-467, 1963.
- [13] A. Cappy, A. Vanoverschelde, M. Schortgen, C. Versnaeyen, and G. Salmer, "Noise Modeling Submicrometer-Gate, Two-Dimensional, Electron-Gas, Field-Effect Transistors," *IEEE Trans. Electron Devices*, vol. Ed-32, p. 2787, December 1985.
- [14] M. Pospieszalski, "Modeling of Noise Parameters of MESFETs and MODFETs and Their Frequency and Temperature Dependence," *IEEE Trans. Microwave Theory Tech.*, vol. 37, no. 9, pp. 1340-1350, September 1989.
- [15] K. Joshin, S. Asai, Y. Hirachi, and M. Abe, "Experimental and Theoretical Noise Analysis of Microwave HEMTs," *IEEE Trans. Electron Devices*, vol. 36, no. 10, pp. 2274-2280, October 1989.

- [16] K. H. G. Duh, P. C. Chao, P. M. Smith, L. F. Lester, B. R. Lee, J. M. Ballingall, and M. Y. Kao, "Millimeter-Wave Low-Noise HEMT Amplifiers," *1988 IEEE MTT-S Digest*, pp. 923-926, 1988.
- [17] P. M. Smith, P. C. Chao, K. H. G. Duh, L. F. Lester, B. R. Lee, J. M. Ballingall, and M. Y. Kao, "Advances in HEMT Technology and Applications," *1987 IEEE MTT-S Digest*, pp. 749-752, 1987.
- [18] S. C. Palmateer, P. A. Maki, W. Katz, A. R. Calawa, J. C. M. Hwang, and L. F. Eastman, "The influence of V:III flux ratio on unintentional impurity incorporation during molecular beam epitaxial growth," *Proc. Gallium Arsenide and Related Compounds Conference 1984* (Inst. Phys. Conf. Series 74), pp. 217-222, 1985.
- [19] P. C. Chao, P. M. Smith, S. C. Palmateer, and J. C. M. Hwang, "Electron-Beam Fabrication of GaAs Low-Noise MESFETs Using a New Tri-Layer Resist Technique," *IEEE Trans. Electron Devices*, vol. ED-22, pp. 1042-1046, 1985.
- [20] K. H. G. Duh, M. W. Pospieszalski, W. F. Kopp, P. Ho, A. A. Jabra, P. C. Chao, P. M. Smith, L. F. Lester, J. M. Ballingall, and S. Weinreb, "Ultra-Low-Noise Cryogenic High-Electron Mobility Transistors," *IEEE Trans. Electron Devices*, vol. ED-35, pp. 249-256, 1988.
- [21] A. Kastarsky and R. A. Klein, "On the low temperature degradation of AlGaAs/GaAs modulation doped field-effect transistors," *IEEE Trans. Electron Devices*, vol. ED-33, pp. 414-423, March 1986.
- [22] K. H. G. Duh, W. F. Kopp, P. Ho, P.-C. Chao, M.-Y. Ko, P. M. Smith, J. M. Ballingall, J. J. Bautista, and G. G. Ortiz, "32-GHz Cryogenically Cooled HEMT Low-Noise Amplifiers," *IEEE Trans. Electron Devices*, vol. ED-36, no. 8, pp. 1528-1535, 1989.
- [23] S. Weinreb and R. Harris, *A 23-GHz Coolable FET Amplifier*, NRAO Internal Report, NRAO, Charlottesville, Virginia.
- [24] P. C. Chao, P. M. Smith, K. H. G. Duh, J. M. Ballingall, L. F. Lester, B. R. Lee, A. A. Jabra, and R. C. Tiberio, "High Performance 0.1 Micron Gate-Length Planar-Doped HEMTs," *1987 IEDM*, paper 17.1, 1987.
- [25] P. Ho, P. C. Chao, K. H. G. Duh, A. A. Jabra, J. M. Ballingall, and P. M. Smith, "Extremely High Gain, Low Noise InAlAs/InGaAs HEMTs Grown by Molecular Beam Epitaxy," *1988 IEDM*, 1988.

Table 1. Performance comparison of conventional AlGaAs/GaAs HEMTs.

Frequency, GHz	Ambient temperature, 300 K			Ambient temperature, 13 K	
	—	8	18	32	
Performance (NF ^a , dB/GA ^b , dB)	gm, mS/mm	NF/GA	NF/GA	NF/GA	T ^c , K/GA
Type A ($1 \times 10^{18}/\text{cm}^3$)	380	0.4/15.2	0.7/11.5	1.3/7.5	5.3/13.9
Type B ($2 \times 10^{18}/\text{cm}^3$)	450	—	0.7/15	1.2/10.0	13.1/14.5

^aNF = noise figure
^bGA = associated gain
^cT = noise temperature

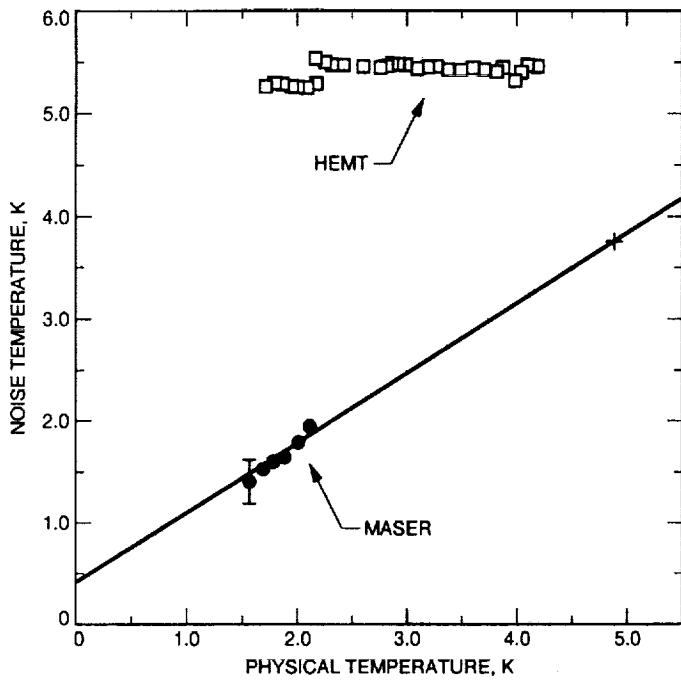


Fig. 1. Noise temperature of an 8.4-GHz ultralow noise maser and HEMT in liquid helium.

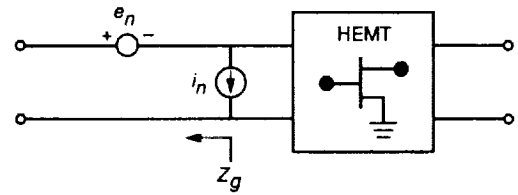


Fig. 3. Noise source representation of a noisy linear two-port circuit.

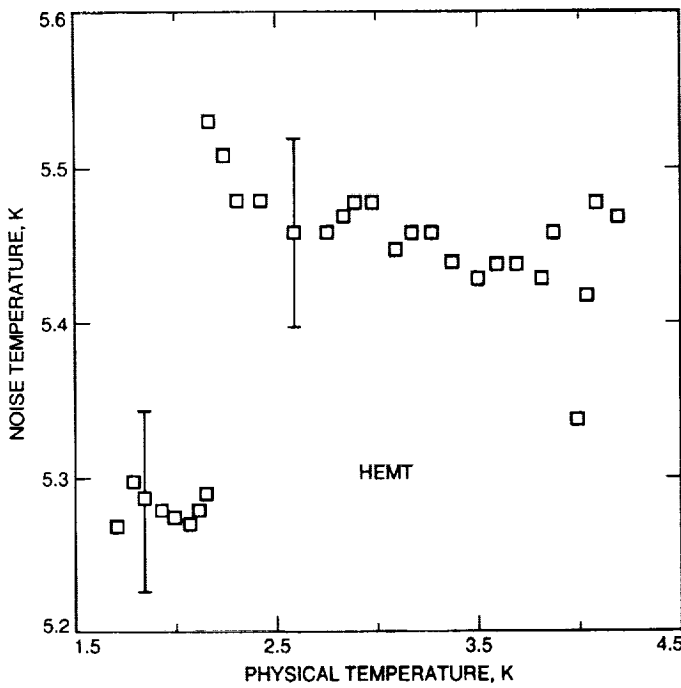


Fig. 2. Noise temperature of an 8.4-GHz HEMT LNA in liquid helium.

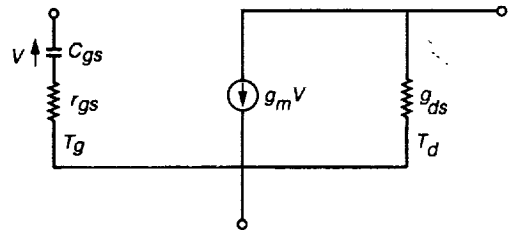


Fig. 4. Pospieszalski HEMT/FET noise model for an intrinsic chip.

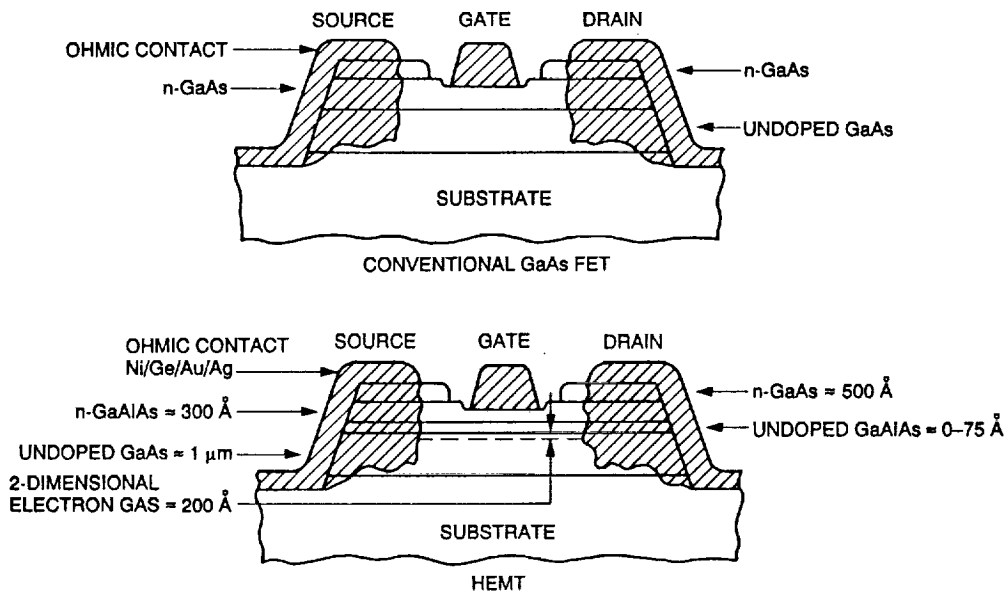


Fig. 5. Representation of MESFET and HEMT device cross-sections.

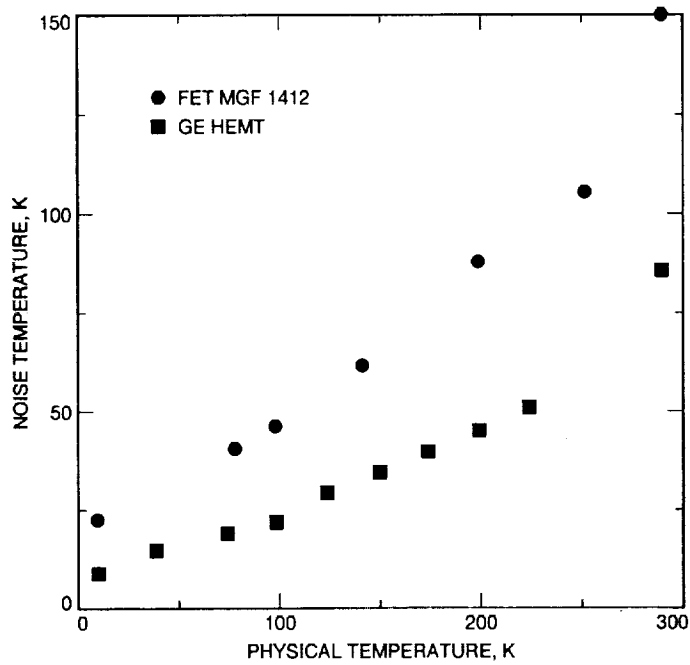


Fig. 6. MESFET versus HEMT noise temperature performance as a function of physical temperature at 8.4 GHz.

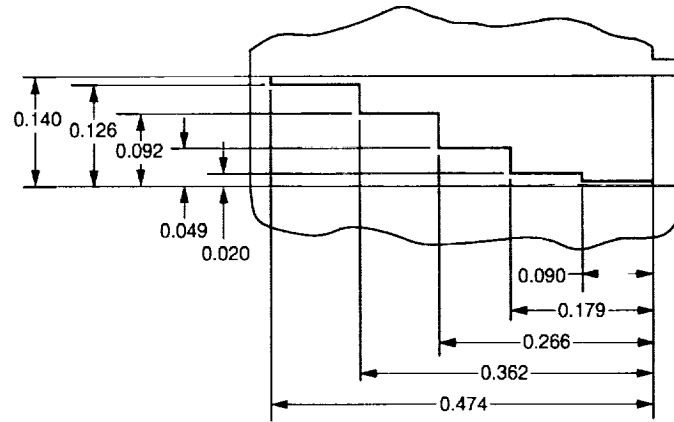


Fig. 7. Ka-band stepped ridge-to-microstrip transition, units in inches.

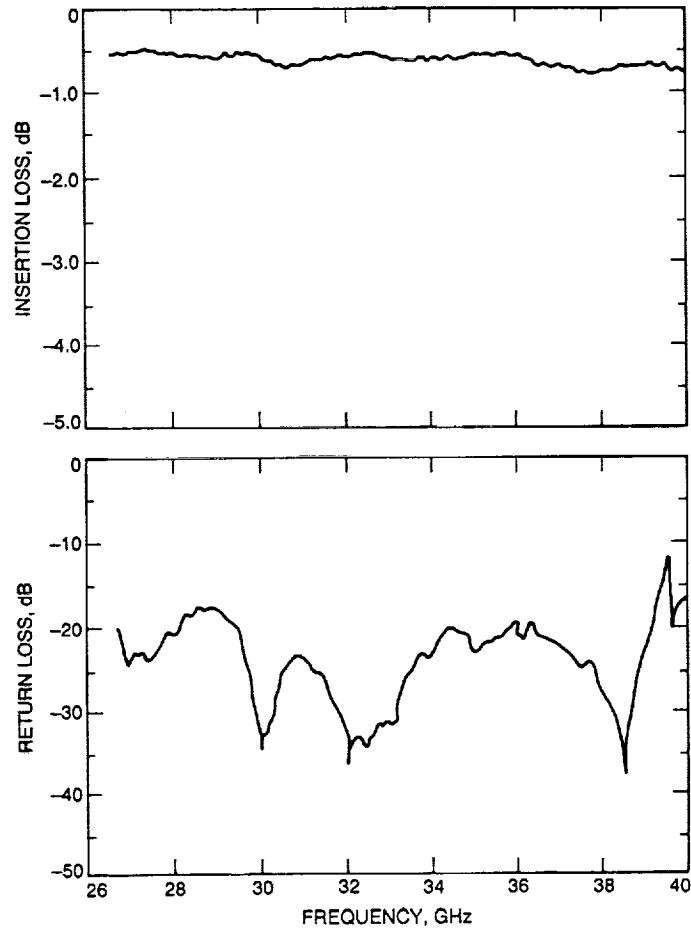


Fig. 8. Measured performance of Ka-band stepped-ridge fixture.

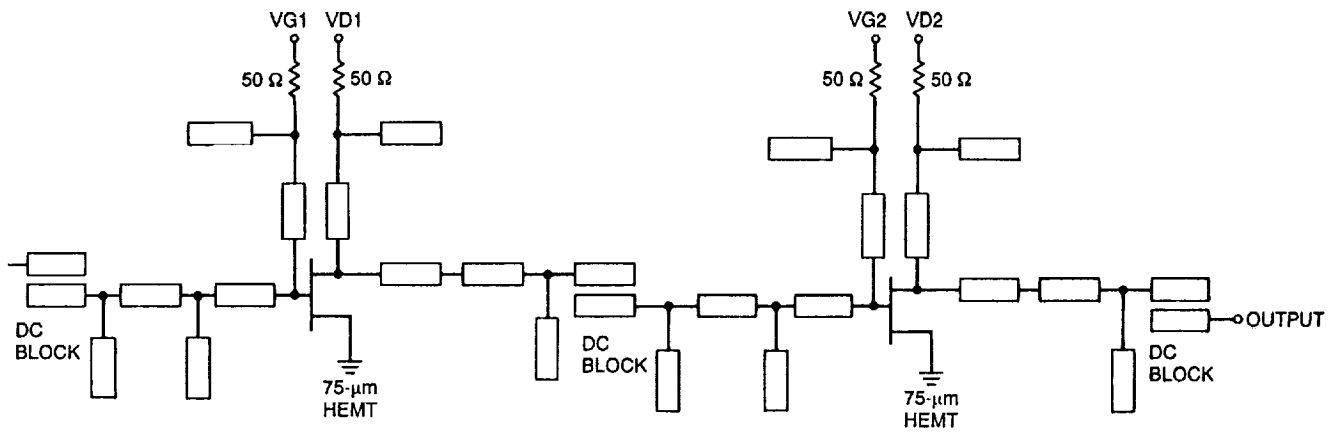


Fig. 9. Two-stage hybrid LNA using 0.25- by 75- μ m HEMTs.

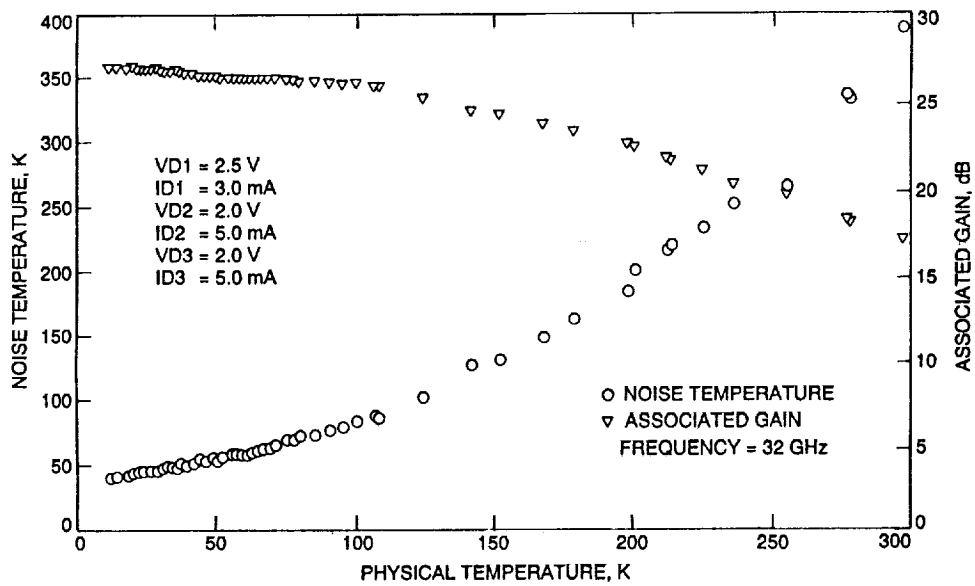


Fig. 10. Three-stage HEMT LNA noise temperature and gain cooling curve.

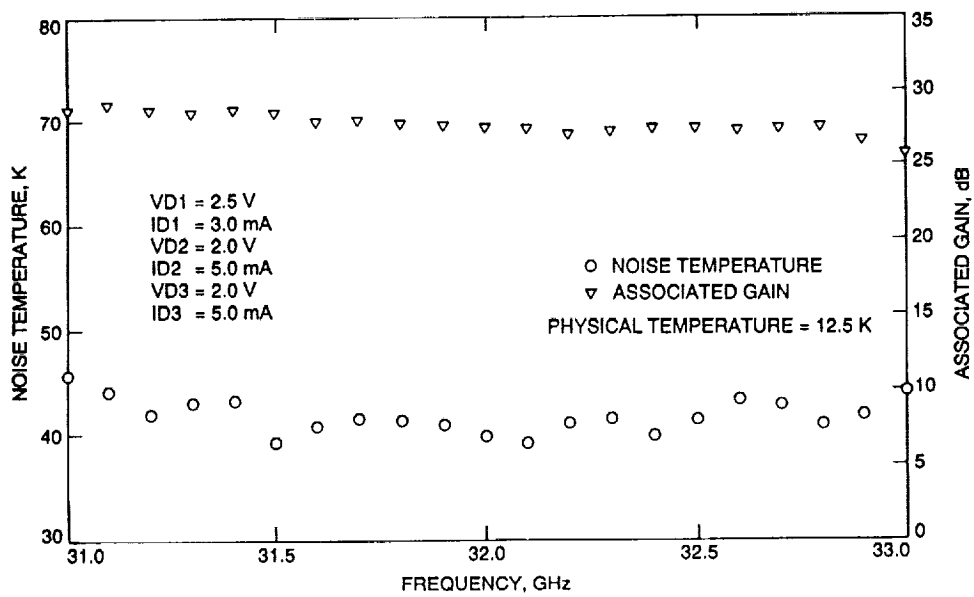


Fig. 11. Three-stage HEMT LNA 12.5-K noise temperature and gain.

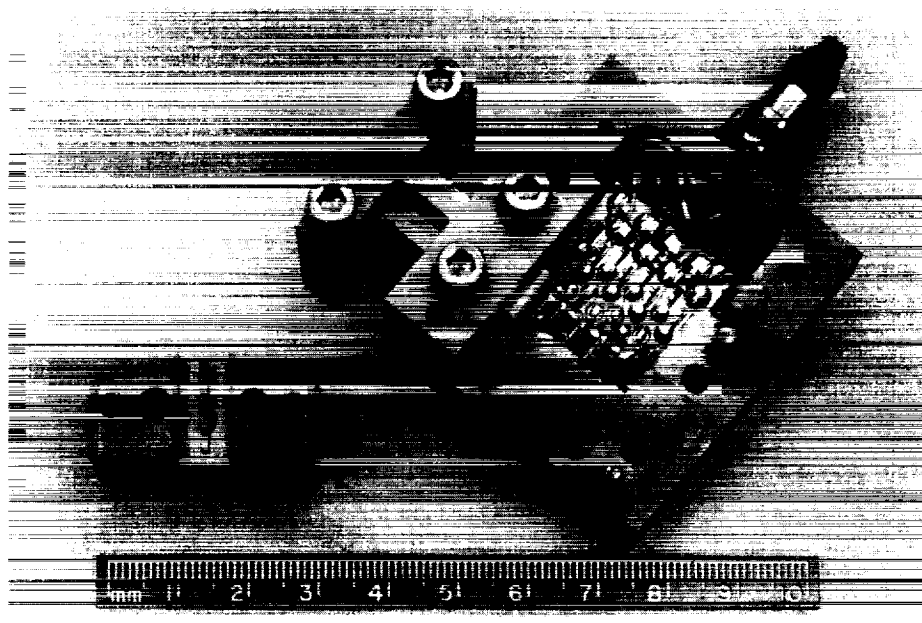


Fig. 12. Four-stage HEMT LNA.

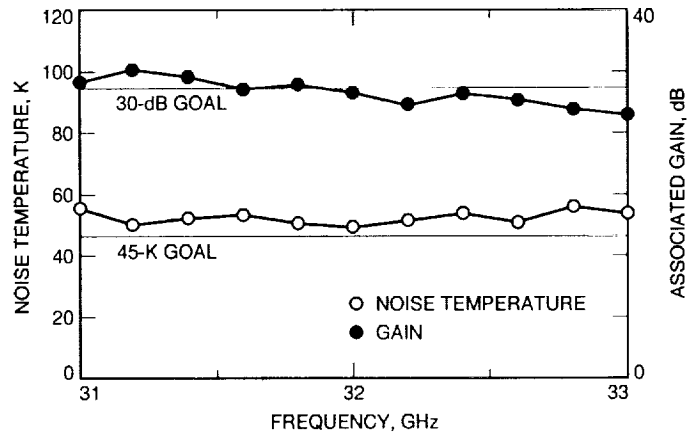


Fig. 13. Cryogenic noise versus gain response of four-stage HEMT LNA.

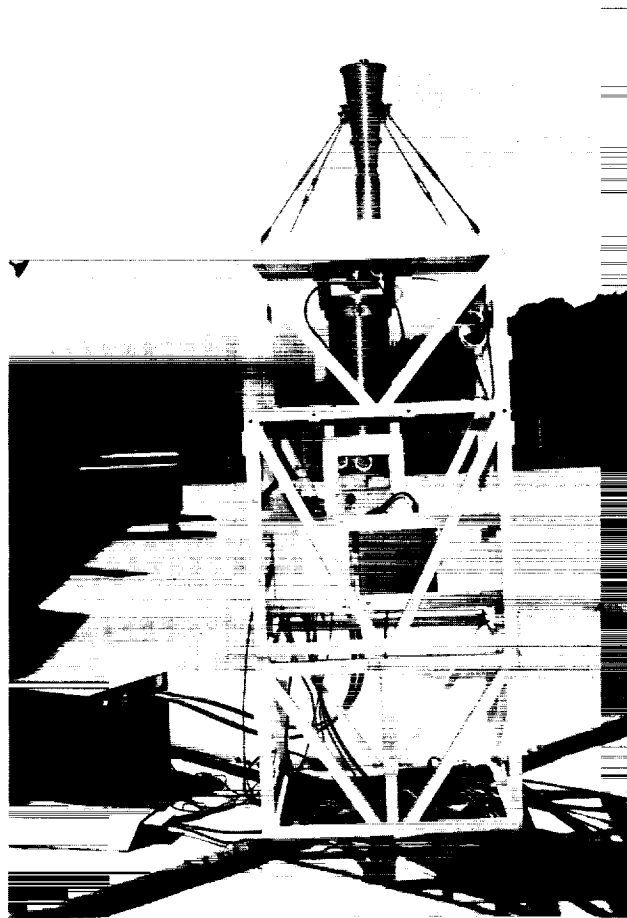


Fig. 14. A 32-GHz HEMT/CCR total power radiometer.

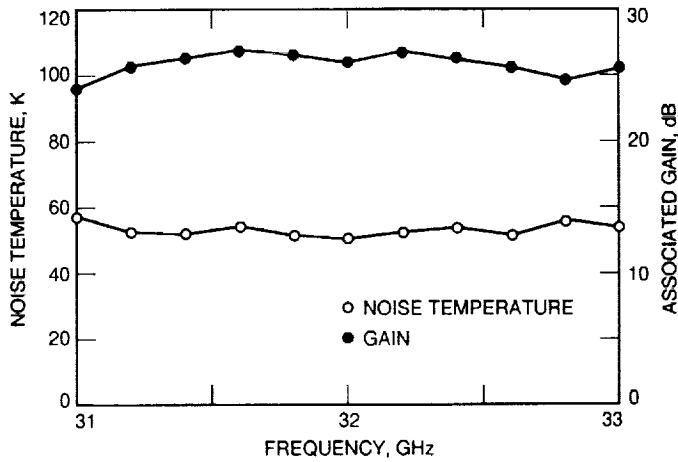


Fig. 15. Noise temperature and gain of 32-GHz HEMT/CCR total power radiometer.

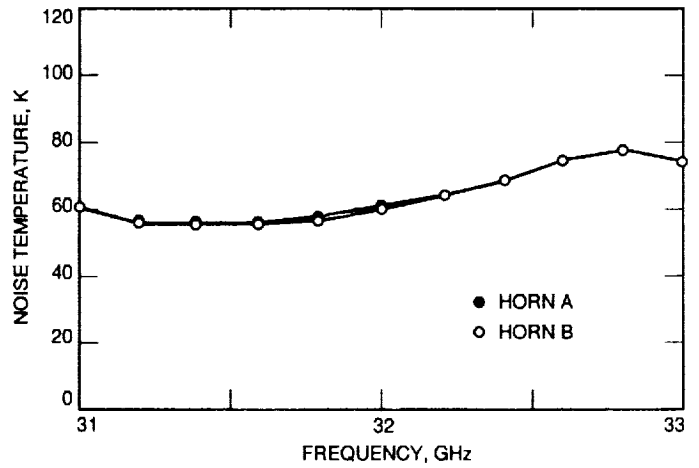


Fig. 17. Noise temperature at horn aperture of 32-GHz HEMT/CCR switching radiometer.

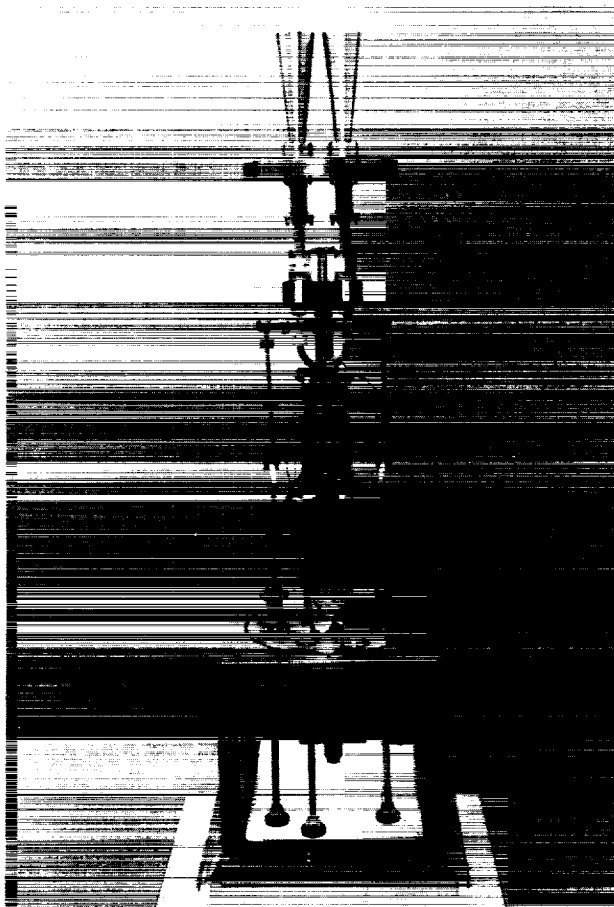


Fig. 16. A 32-GHz HEMT/CCR Dicke-switching radiometer without radiation shields and vacuum jacket.

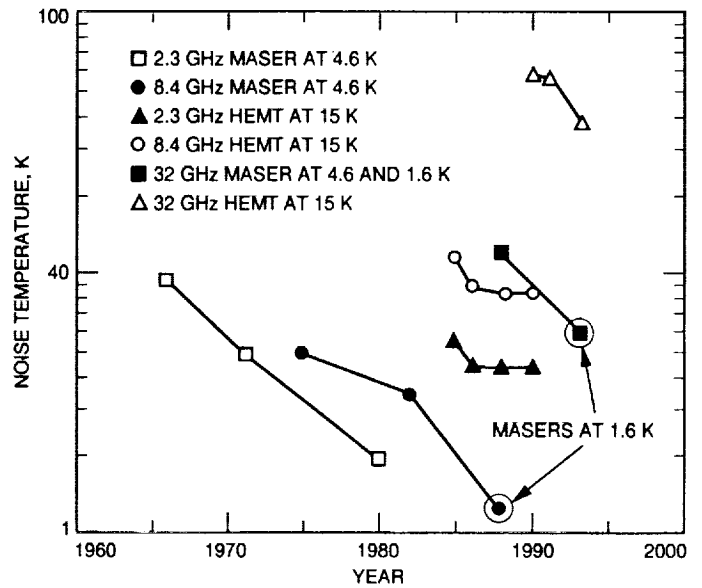


Fig. 18. Evolution of low noise performance of maser and HEMT amplifier systems.